EXCIPLEX LASER KINETICS

C. Duzy, J. H. Jacob, A. Mandl, et al.
Avco Everett Research Laboratory, Inc.
2385 Revere Beach Parkway
Everett MA 02149

Final Technical Report for Period 1 March 1978 to 29 September 1979

Sponsored by
DEFENSE ADVANCED RESEARCH PROJECTS AGENCY
DARPA Order No. 3500

Monitored by
OFFICE OF NAVAL RESEARCH
DEPARTMENT OF THE NAVY
Arlington VA 22217

FOREWORD

DARPA Order No.: 3500

Program Code No.:

Name of Contractor: Avco Everett Research Laboratory, Inc.

Effective Date of Contract: 1 March 1978

Contract Expiration Date: 29 September 1979

Amount of Contract: $265,456

Contract No.: N00014-78-C-0334

Principal Investigator and Phone No.: D. Trainor
(617) 389-3000, Ext. 467

Scientific Officer: Director, Physics Program,
Physical Sciences Div.
Office of Naval Research
Department of the Navy
800 North Quincy Street
Arlington, VA 22217

Short Title of Work: Exciplex Laser Kinetics

Reporting Period: Final Technical Report

UNCLASSIFIED

SECURITY CLASSIFICATION OF THIS PAGE (When Data Entered)

REPORT DOCUMENTATION PAGE		READ INSTRUCTIONS BEFORE COMPLETING FORM
1. REPORT NUMBER	2. GOVT ACCESSION NO.	3. RECIPIENT'S CATALOG NUMBER
4. TITLE (and Subtitle) Exciplex Laser Kinetics		5. TYPE OF REPORT & PERIOD COVERED Final Technical Report 1 Mar 1978 — 29 Sep 1979
		6. PERFORMING ORG. REPORT NUMBER
7. AUTHOR(s) C. Duzy, J.H. Jacob, A. Mandl, A.K. Medhekar, J.H. Parks, M. Rokni, V.H. Shui and D.W. Trainor		8. CONTRACT OR GRANT NUMBER(s) N00014-78-C-0334 DARPA Order-3500
9. PERFORMING ORGANIZATION NAME AND ADDRESS Avco Everett Research Laboratory, Inc. 2385 Revere Beach Parkway Everett, MA 02149		10. PROGRAM ELEMENT, PROJECT, TASK AREA & WORK UNIT NUMBERS
11. CONTROLLING OFFICE NAME AND ADDRESS Defense Advanced Research Projects Agency DARPA Order No. 3500		12. REPORT DATE November 1979 13. NUMBER OF PAGES 44
14. MONITORING AGENCY NAME & ADDRESS(if different from Controlling Office) Office of Naval Research Department of the Navy Arlington, VA 22217		15. SECURITY CLASS. (of this report) Unclassified 15a. DECLASSIFICATION/DOWNGRADING SCHEDULE

16. DISTRIBUTION STATEMENT (of this Report)

Approved for Public Release; Distribution Unlimited.

17. DISTRIBUTION STATEMENT (of the abstract entered in Block 20, if different from Report)

18. SUPPLEMENTARY NOTES

19. KEY WORDS (Continue on reverse side if necessary and identify by block number)

Visible Lasers
Mercury Halide Lasers
Mercury Halide Kinetics
HgCl* and HgBr* Lasers
Three-Body Quenching Kinetics
Heterogeneous Surface Reactions

20. ABSTRACT (Continue on reverse side if necessary and identify by block number)

This contract was undertaken to obtain useful kinetic information necessary to evaluate various laser candidates with regard to their application as efficient, scalable laser systems. Historically, our approach at AERL involved developing a kinetic data base using as input the results of small-scale experiments and theoretical calculations, followed by laser code modeling of medium-scale laser experiments. In this way, a reliable, accurate model for the KrF* laser (249 nm) has evolved. Under this contract,

DD FORM 1 JAN 73 1473 EDITION OF 1 NOV 65 IS OBSOLETE

UNCLASSIFIED

SECURITY CLASSIFICATION OF THIS PAGE (When Data Entered)

(20)
kinetic information on XeF* (351 nm) HgCl* (558 nm), HgBr* (502 nm), ArF* (193 nm) as well as KrF* was collected. This includes heavy particle quenching of HgX*, three-body quenching of various rare gas halides and an experimental determination of the heterogeneous reactions producing $HgCl_2$.

REPORT SUMMARY

This contract was undertaken to obtain useful kinetic information necessary to evaluate various laser candidates with regard to their application as efficient, scalable laser systems. Historically, our approach at Avco Everett Research Laboratory, Inc. (AERL) involved developing a kinetic data base using as input the results of small-scale experiments and theoretical calculations, followed by laser code modeling of medium-scale laser experiments. In this way, a reliable, accurate model for the KrF* laser (249 nm) has evolved. Under this contract, kinetic information on XeF* (351 nm), HgCℓ (558 nm), HgBr* (502 nm), ArF* (193 nm) as well as KrF* was collected. This includes heavy particle quenching of HgX*, three-body quenching of various rare gas halides and an experimental determination of the heterogeneous reactions producing $HgC\ell_2$.

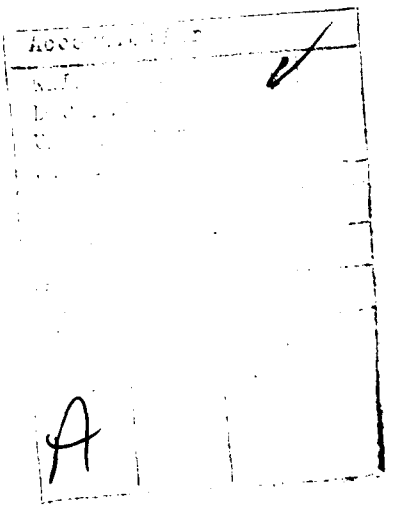

TABLE OF CONTENTS

LIST OF ILLUSTRATIONS

I. INTRODUCTION

The tasks completed under this contract were performed by a variety of research scientists utilizing equipment especially chosen to facilitate the successful completion of each task. Many of the experimental devices were constructed or modified specifically to be utilized on this contract. The systems chosen for study included the mercury halide laser candidates, KrF*, ArF* and XeF*. Much of the information we obtained is in the form of rate constants describing various formation or quenching reactions important in these exciplex laser systems, i.e.,

〈i〉 Surface Catalyzed Reaction (Experimental)

$$Hg + C\ell_2 \xrightarrow{\text{Surface}} HgC\ell_2$$

〈ii〉 Two-Body Quenching Reactions (Experimental)

$$HgC\ell^* + Q \rightarrow \text{Products}$$

$$HgBr^* + Q \rightarrow \text{Products}$$

〈iii〉 Three-Body Quenching Reactions (Theoretical)

$$RgX^* + Q + M \rightarrow \text{Products}$$

The results of our studies on these processes are summarized in this final report.

Earlier work on mercury halide quenching completed under this contract has been included as part of an Interim Technical report and recently published in the open literature.[1,2] The reader is referred to these sources.

II. RESULTS

A. SURFACE CATALYZED REACTION OF MERCURY AND CHLORINE

The science community has seen a rapid growth in the variety of high-power, electronic transition lasers available which radiate throughout the ultraviolet and visible wavelength region of the spectrum.[3] Notable among these is the mercury chloride laser operating in the green near 558 nm.[4] This compound was produced in an e-beam excited mixture of Ar, Xe, Hg and $CC\ell_4$ operated at elevated temperature to allow for adequate densities of mercury to be obtained. Using this method of excitation, production of HgX* proceeds primarily via an ion-ion formation channel. This expenditure of > 25 eV of energy to produce an electron ion pair to produce a visible (~ 2.5 eV) photon is wasteful from an energy efficiency perspective. It would clearly be better to produce the low-lying Hg* (^3P) states and allow the reaction to proceed via a charge transfer (harpooning) reaction. These excited mercury atoms can be efficiently created in a discharge. Unfortunately, formation via this metastable channel places a restriction on the bond strength of the halogen donors; namely, it must be sufficiently weak, so that the excited mercury atoms have sufficient energy to break the bond and be able to energetically access the HgX*(B) upper laser level in the reactive encounter. Most e-beam discharge experiments to date have explored the use of molecular chlorine,

$C\ell_2$, as the halogen fuel.[5] Unfortunately, early attempts to produce efficient lasing were not very successful,[5] in that the reactants were rapidly disappearing upon entering the heated laser cavity before any exciting e-beam sustained discharge could be applied.

To investigate this phenomena, facilitate data collection and permit more direct experimental information to be gathered, we designed and fabricated a simple experimental facility to research this apparent reaction of mercury and chlorine at elevated temperatures. These experiments showed the reaction as proceeding on the walls of the container with a stoichiometric loss of Hg and $C\ell_2$, e.g.,

$$nHg + nC\ell_2 \xrightarrow{\text{walls}} (HgC\ell_2)_n$$

Data were collected in Inconel, quartz, stainless steel, and Teflon-coated stainless steel reaction cells. The results of these experiments in turn prompted the laser experiments to decrease the residence time in the cavity to times < 10 s. Subsequently, intrinsic laser efficiencies in excess of 3% were obtained[6] for $HgC\ell^*$ lasers compared to the earlier efficiencies reported[5] of < 1%.

1. Experimental

The experimental apparatus used to measure these effects is shown schematically in Figure 1; it consisted of four main units:

a) The test cells (quartz, Inconel, stainless steel, Teflon-coated stainless steel).

b) Reactant reservoirs (containing the Hg and $C\ell_2$/ buffer mixtures).

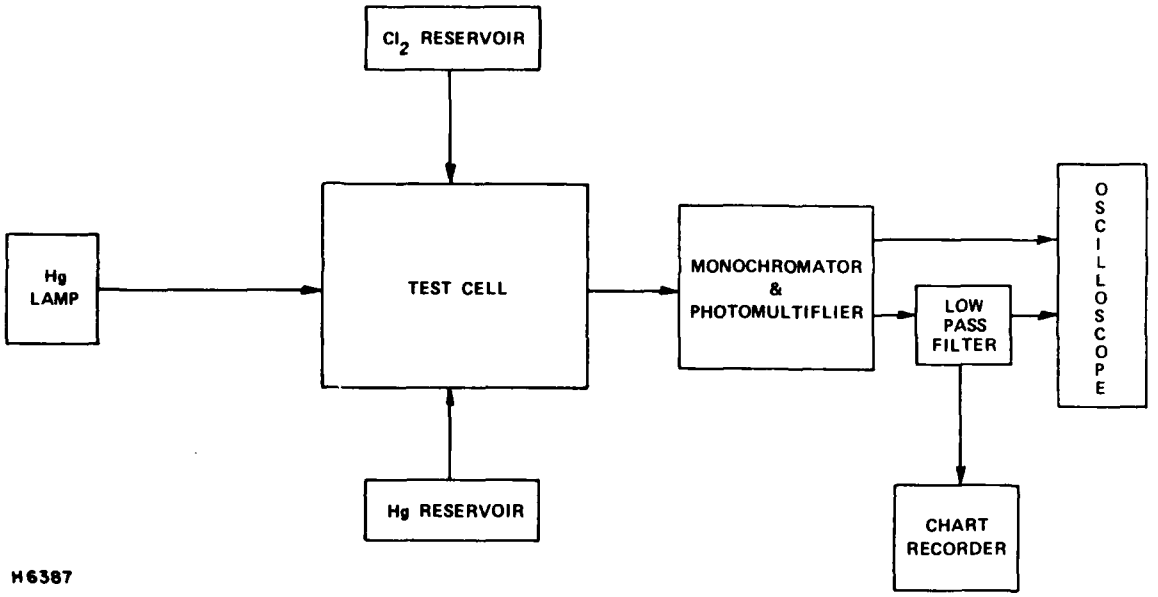

Figure 1 Schematic Diagram of the Apparatus

c) The heating and temperature control.

d) The data monitoring equipment.

a. The Test Cells

The cells consisted of a cylindrical cavity made of the various materials investigated and fitted at each end with quartz windows to enable absorption experiments to be conducted as a function of time. (Typical dimensions for two of the cells are shown in Figure 2.) A gas-line port is provided in the center of each cell to provide entry of the reactant gases. Once the gases are admitted to the cell, they are sealed by a heated valve fitted at the top of the addition inlet.

b. Reactant Gas Handling

The mercury (Fisher Scientific, triple distilled) was stored in a heated reservoir with separate temperature controls. Chlorine (Matheson, research grade, 99.96%) was also stored in a separate reservoir as a 5 or 2.5% mixture in argon (Scientific Gas Products, high purity 99.995%). The density of the mercury was determined from published vapor pressure data[7] and the temperature of the mercury vessel. The chlorine density was determined from pressure measurements of the mix before placement into the cell and by absorption experiments performed in-situ.

c. Heating and Temperature Control

Typical operating temperatures were near 525°K. Under these conditions, convenient reaction rates could be detected ($t_{reaction}$ ~ 1 min) and successfully monitored. Thermocouples were used to monitor the temperature at various component locations and thereby

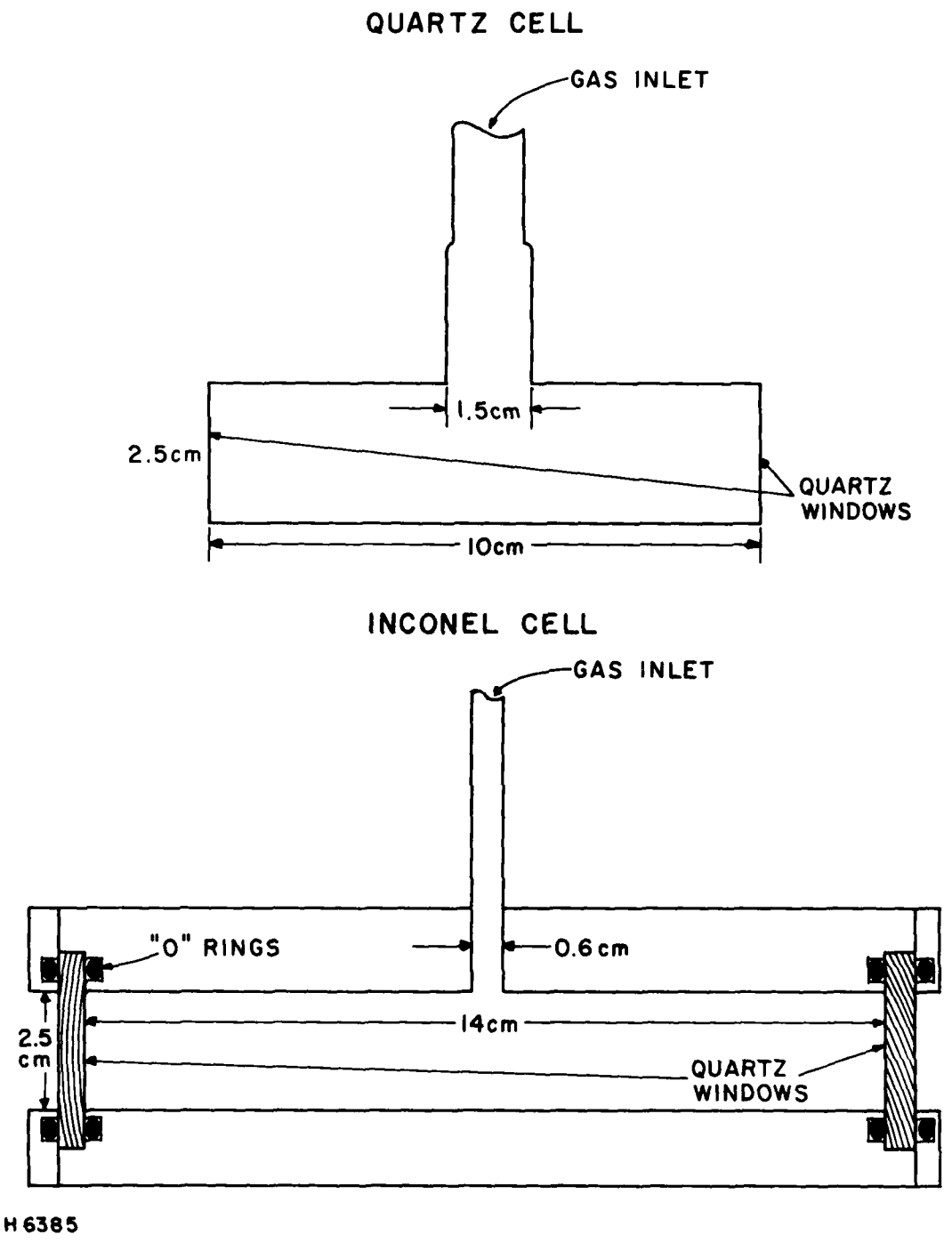

Figure 2 Typical Cell Dimensions (Quartz and Inconel)

insured that no cold spots were present. The cell and reservoirs were heated through contact with resistively heated elements such as standard heating tapes. The entire system was thoroughly shielded and insulated to allow for maximum temperature uniformity.

d. Data Monitoring

The light source consisted of a low-pressure mercury pen lamp (Oriel, Type C) emitting a variety of atomic mercury spectral lines. The particular line monitored was isolated by a 1/2-m monochromater (Jarrell-Ash) and its intensity related to the output of photomultiplier tube (IP28). The latter was recorded by a calibrated strip chart recorder (MFE, Model M22C-AMA).

2. Procedure

The procedure was to follow the quantitative disappearance of the chlorine as a function of time by monitoring either the 313 or 366 nm lines from the pen lamp. In the absence of mercury in the reaction cell, the change in transmission from that through the empty cell to that with the chlorine/argon mix present, allowed a measurement of the chlorine present through use of Beer's law and the known extinction coefficient for chlorine.[8] This was compared to that expected from the total pressure and the percentage of chlorine in the mix. The agreement was within 10%.

3. Results and Discussion

Typical signals for an Inconel cell at 250°C are shown in Figure 3. The upper trace is for the 3662 Å Hg line transmission. The cell is initially evacuated to ~ 1 μ and I_o established. $C\ell_2$ (= 7.2×10^{17} cm^{-3}) is then added with an Ar diluent to a total

pressure of 0.95 atm. The transmitted signal is observed to immediately drop to a lower value consistent with the amount of $C\ell_2$ added. The lamp is then blocked to establish a zero. The cell is again evacuated and as one would expect the transmitted signal returned to I_o. Hg (= 3.6×10^{17} cm^{-3}) is then added with no change in the 3662 Å transmission signal since ground-state Hg does not absorb at this wavelength. When $C\ell_2$ (= 7.2×10^{17} cm^{-3}) is again added, the signal drops to the value first observed but is then seen to decay ($\sim$ 50 s) to a value consistent with a $C\ell_2$ density of 3.5×10^{17} cm^{-3}. This would imply that 3.7×10^{17} cm^{-3} of $C\ell_2$ has disappeared.

The bottom trace shows similar data involving the transmission of 2537 Å radiation. Since ground-state Hg absorbs 2537 Å radiation, this trace indicates the fate of the Hg. The cell is initially evacuated ($\sim$ 1 μ). Hg (= 3.6×10^{17} cm^{-3}) is then added and one observes a dramatic drop in the transmitted signal, however it does not go to zero. (This is because the source linewidth is broader than the Hg absorption linewidth, and so there is weakly attenuated transmission in the wings of the 2537 Å line. In other experiments, we have shown that if a nonabsorbing buffer gas at $\sim$ 1 atm is added to the Hg, the Hg absorption linewidth is pressure broadened and the transmitted signal does indeed go to zero). A mixture of $C\ell_2$ and Ar was then added. We observe that the transmitted signal increases indicating that all the Hg has reacted in a time also of $\sim$ 50 s.

It is observed that the transmitted signal at the end of the trace is greater than the initial I_o. This is probably due to residual mercury being present in the cell after evacuation to ~ 1 μ pressure. The absorption coefficient for the 2537 Å transition in Hg is so large, that very low densities of Hg ($10 - 10^{11}$ cm^{-3}) are detectable in absorption.[9] By using the data from the top and bottom traces of Figure 3, one can deduce that for every Hg reacted a $C\ell_2$ reacted. Thus

$$nHg + nC\ell_2 \Longrightarrow (HgC\ell_2)_n$$

where $n \geq 1$.

Measurements similar to the ones given in Figure 3 were repeated at higher diluent pressure (p = 2 atm) and are shown in Figure 4. Once again, it is observed that the ratio of the reacted Hg to reacted $C\ell_2$ is unity. The only difference is that the reaction time has approximately doubled (i.e., 90-95 s). This is consistent with a diffusion limited reaction occurring on the walls of the container.

It can be shown that the diffusion time, τ_d, varies linearly with pressure[10] and with the square of a critical dimension of the vessal. Thus, a reaction which is wall-dominated will be slowed directly as the pressure is increased, whereas a two-body homogeneous reaction rate would be unchanged as the diluent pressure is increased and a three-body homogeneous reaction rate would increase with increasing third-body pressure. Similarly, in other experiments, the cell diameter was increased and the reaction rate was

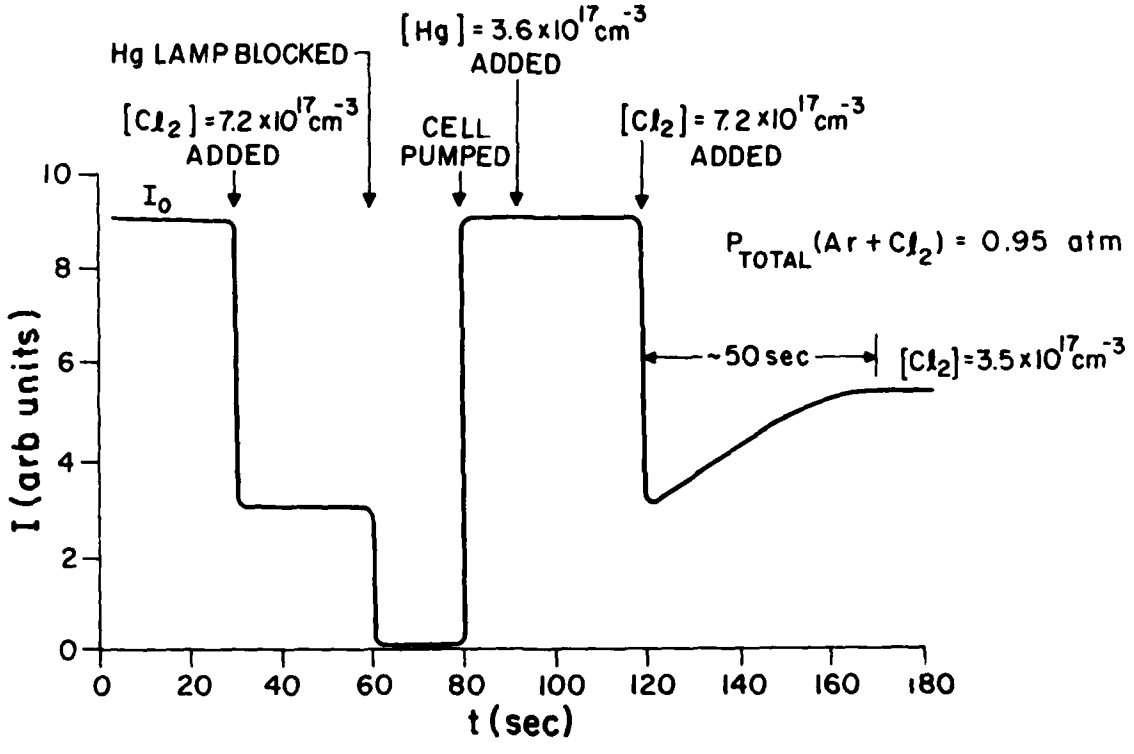

Figure 3a Chlorine Absorption Data at 3662 Å in an Inconel Cell at T = 250°C and p = 0.95 amg

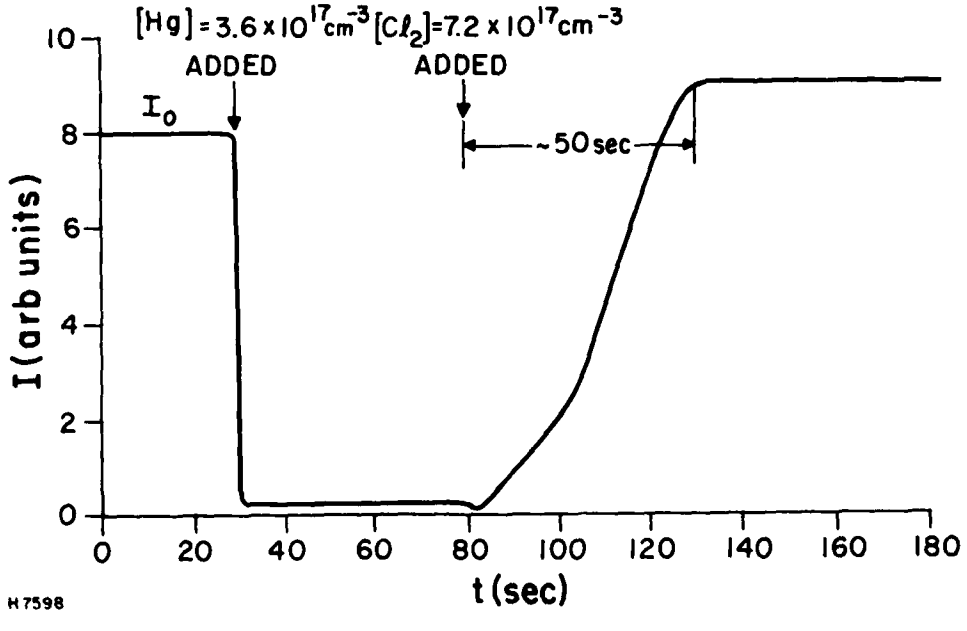

Figure 3b Mercury Absorption Data at 2537 Å in the Same Cell Under the Same Conditions as in (a)

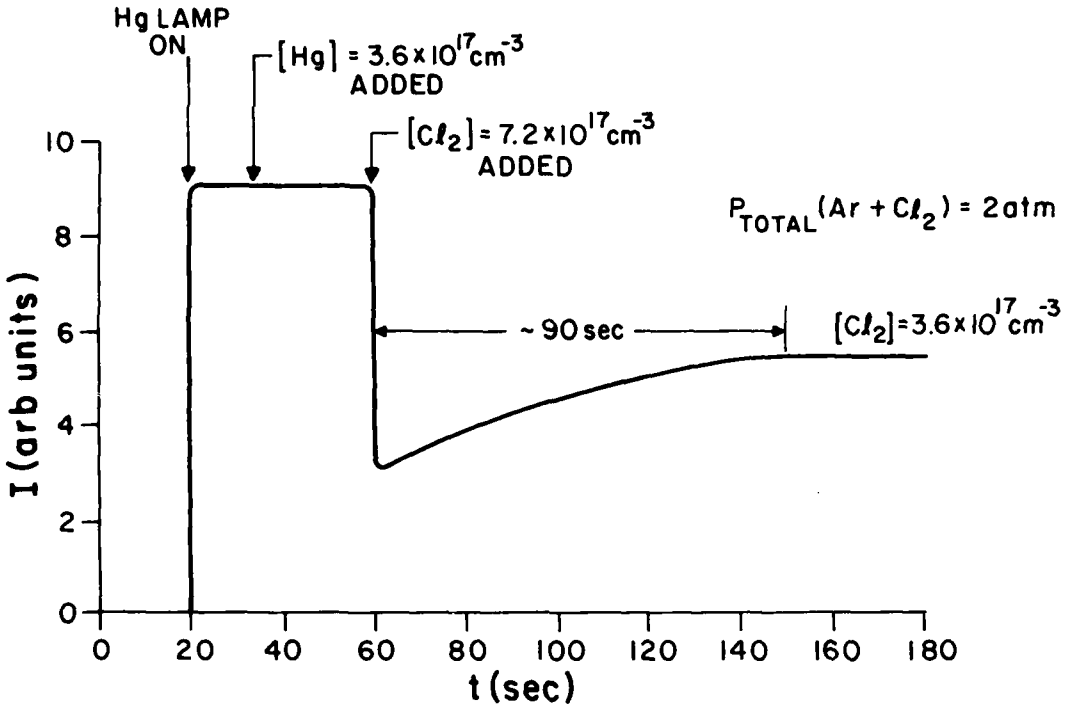

Figure 4a Chlorine Absorption Data at 3662 Å in an Inconel Cell at T = 250°C and p = 2.0 amg

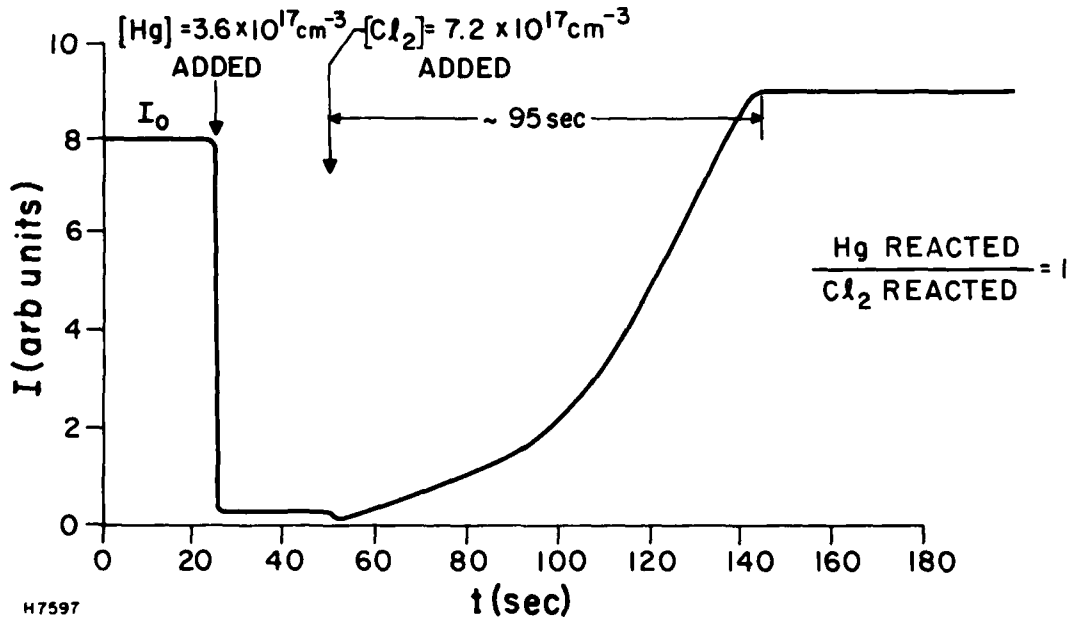

Figure 4b Mercury Absorption Data at 2537 Å in the Same Cell Under the Same Conditions as in (a)

also observed to decrease. This is also consistent with the diffusion model, since as the cell diameter is increased, the reaction rate should similarly decrease for a diffusion dominated heterogenerous surface reaction. It is therefore likely that Hg and $C\ell_2$ react heterogeneously at elevated temperatures ($T \sim 250°C$) to form a compound with a stoichiometric formula $(HgC\ell_2)_n$.

It was also observed that after several runs the reaction rate became faster until it eventually became independent of the wall material. Thus, whether one started with Inconel (which seemed to initially give the best results) or any other of the materials tested, the heterogeneous reaction rate approached the same value after a few runs. It seems likely that the reaction products formed on the surface eventually dominate the surface chemistry.

Our initial observations, however, were that Inconel was less reactive than quartz which was less reactive than stainless steel, all of which were less reactive than the product coated surface. These materials are typically found in e-beam discharge laser cavity devices.

Experiments which we hoped would significantly alter the observed catalytic removal of mercury and chlorine were also performed. These involved the addition of oxidizing agents, such as O_2 or F_2 to the hot reaction cells to passivate the cell's surfaces, hopefully reducing its reactivity. These experiments showed little effect. Our observations were again consistent with the view that the pristene reactivity of the surface was initially significant and perhaps different one surface from another, but quickly cell surfaces

approached some common level of reactivity. It is likely that ($HgC\ell_2$) eventually coats the surfaces[11] and this makes all surfaces essentially the same.

B. HEAVY PARTICLE QUENCHING OF HgCℓ* AND HgBr*

In addition to the very practical constraints imposed by the surface catalyzed reaction described in Section II-A, there remain a number of kinetic issues that effect the scalability of the mercury halide laser candidates. These include the formation and quenching kinetics of the upper laser level, absorption of the active media and depopulation of the lower laser level. Under this contract, we have designed and fabricated an experimental facility to study the heavy-particle quenching of the mercury halide upper laser levels.[1] Using this equipment, many of the needed rate constants have been measured. Some rate data have been published[2] and summarized in our earlier Interim Technical report. In this report, measurements of the rates of collisional quenching of HgCℓ* ($B^2\Sigma^+_{1/2}$) by He, Ne, Ar, Kr, Xe and N_2 at pressures up to 3000 torr, and HgBr* ($B^2\Sigma^+_{1/2}$) by He, Ar, Xe, N_2, Br_2, HBr, CF_3Br and $CC\ell_3Br$ at pressures up to 1000 torr are reported. Steady-state measurements were made of HgCℓ* and HgBr* fluorescence produced by photolyzing $HgC\ell_2$ and $HgBr_2$, respectively, using Xe_2* radiation. A modified Stern-Volmer analysis was used in determining the rates. This analysis accounts for absorption of Xe_2* radiation measured for the quenching species $C\ell_2$, $HC\ell$, $CC\ell_4$, Br_2, HBr, CF_3Br and $CC\ell_3Br$. The measured vacuum ultraviolet cross sections for these species are also included.

Mercury chloride and mercury bromide are currently candidates for efficient high-power visible lasers. In order to optimize the efficiency of these laser systems, a detailed knowledge of the heavy-particle quenching kinetics is important. These quenching kinetics enable one to choose the appropriate laser gas mixtures and, in addition, to determine the saturation flux. The upper laser level $B^2\Sigma^+_{1/2}$ of the mercury monohalides is an ion pair state which is connected by a large transition moment to the lower level $X^2\Sigma^+_{1/2}$. Recently measurements of HgCℓ* quenching have been reported[2] for pressure below 1000 torr. In that study only an upper bound for the quenching rates by He, Ar and N_2 could be determined since three-body reactions were not observed in that pressure range. We are now able to report measurements of HgCℓ* quenching by He, Ne, Ar, Kr and N_2 extending to pressures of 3000 torr. The quenching by Xe was also measured at these higher pressures and a three-body quenching rate was determined. Measurements were also made of the quenching of HgBr* by He, Ar, Xe, N_2, Br_2, HBr, CF_3Br and $CC\ell_3Br$. These measurements were made at pressures below 1000 torr. The quenching rates were obtained for both mercury monohalide excited states by analyzing the steady-state dependence of HgX* (X = Cℓ, Br) fluorescence intensity on the partial pressure of the quenching gas.

1. Approach

HgX is produced in the excited state $B^2\Sigma^+_{1/2}$ by optically pumping HgX_2 vapor. Wieland has shown[12] that absorption at

λ = 1800 Å and 1950 Å maximizes the production of HgCℓ* ($B^2\Sigma^+_{1/2}$) and HgBr* ($B^2\Sigma^+_{1/2}$), respectively. These states have been identified as the upper laser levels. The optical pumping source was peaked around 1800 Å (1950 Å) to reduce the possibility of producing additional excited HgCℓ(HgBr) higher lying electronic states. It is essential to avoid populating the B states via radiative cascade processes which could vary in the presence of quenching gases. The immediate photodissociation of HgX_2 is assured since no evidence has been observed[13] to indicate intermediate states. Spontaneous emission from the excited HgCℓ* or HgBr* molecule in the B-X band lies between 5600 and 3400 Å and is used to monitor the excited state density. The radiative lifetimes of the HgCℓ* and HgBr*, B states have recently been measured by Eden[14] as 22.2 ns and by Djeu and Mazza[15] as 23.2 ns, respectively.

Collisions of HgX* with either a parent HgX_2 molecule or an added quenching molecule, Q, can deactivate the excited state prior to emission. As will be shown below, a modified Stern-Volmer analysis applied to the variation of emission intensity with pressure of the additive gas allows one to determine the quenching rate constants for various gas species. This optical pumping technique avoids any ambiguities which might be introduced by the presence of electrons. A schematic diagram of the experimental apparatus is shown in Figure 5 and is described in detail elsewhere.[1]

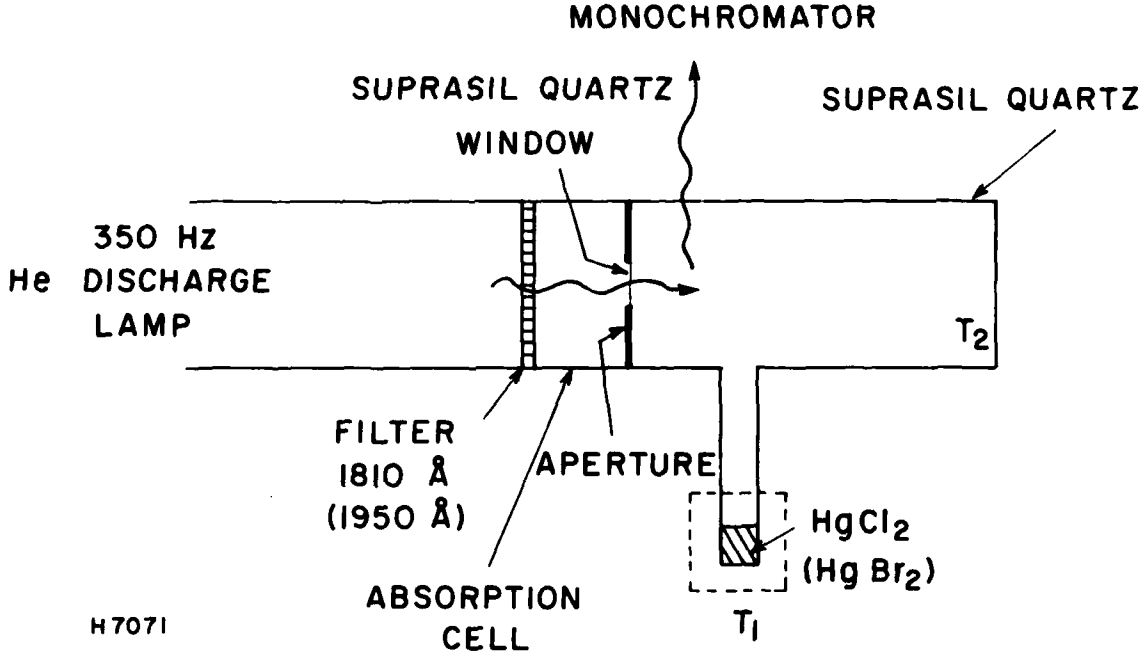

Figure 5 Experimental Apparatus for Quenching Measurements

Briefly, a xenon-discharge lamp is used to produce HgX* in the reaction cell by photolyzing HgX_2 salts. An absorption cell located between the lamp and reaction cell is used in additional experiments to measure the absorption cross sections of the various quenching gases at the excitation wavelength. In this experimental configuration the absorption at 1800 Å (1950 Å) is measured by filling the absorption cell with the quenching gas and monitoring the resulting decrease in HgCℓ* (HgBr*) fluorescence. The need for these absorption cross sections will be discussed below. All the components between the lamp and the reaction cell are closely coupled to each other, minimizing intermediate air spaces and the resulting vacuum ultraviolet absorption by O_2. The end of the absorption cell closest to the reaction cell is apertured to a diamter of ~ 6 mm to reduce wall effects such as scattering. This results in a faint 6 mm diameter column of HgX* flurorescence radiation visible in the reaction cell. As shown in Figure 5 the reaction cell sample arm is kept at a lower temperature, T_1, than the cell body, T_2, to avoid HgX_2 condensation on the cell windows. The xenon flashlamp is pulsed at ~ 350 Hz and the HgX* fluorescence signal is averaged using standard techniques.

It was shown previously that a buffer gas of Xe > 100 torr is necessary to ensure that the vibrational manifold of the excited HgX* ($B^2\Sigma^+_{1/2}$) level is relaxed. This relaxation can be quite rapid since the vibrational energy spacing is ~ 190 $cm^{-1} \leq kT$. Assuming that relaxation is occurring on a time scale comparable to the radiative lifetime, provides an estimate of the two-body

rate constant for vibrational relaxation of $\sim 10^{-11}$ cm^3 s^{-1}. This ensures that the vibrational relaxation of the upper state manifold is comparable or faster than the quenching rate expected in higher pressure gas mixtures.

It was also shown[2] that the ratio, R, of the fluorescence signal without quenching to that with, multiplied by $e^{-\alpha}$ (where α is the absorption coefficient of the quenching gas) when plotted against the quenching gas density, [Q], results in a straight line of slope $k_Q\tau$. This is the expected behavior expressed by the modified Stern- Volmer relation

$$Re^{-\alpha} = 1 + k_Q\tau\ [Q] \qquad (1)$$

At the photolysis wavelengths used (i.e., 1800 and 1950 Å) the rare gases do not absorb ($\alpha = 0$) and Eq. (1) reduces to the standard Stern-Volmer expression. All the quenching data presented below were taken with at least 100 torr of Xe present to ensure that upper laser level was vibrationally relaxed.

2. Data

The measurements on the quenching of HgCl* by the rare gases and N_2 have been extended to pressures of 3000 torr. Quenching by the rare gases Ne and Kr have also been included. The measured values $k_Q\tau$ and the derived rate constant k_Q using τ = 22.2 ns are listed in Table I. The measurements at higher pressures have enabled us to determine actual quenching rates for all the rare gases as opposed to the upper bounds previously[2] estimated for He, Ar and N_2. The overall uncertainty in these values is ± 25%.

TABLE I

$HgC\ell^*$ ($B^2\Sigma^+_{1/2}$) QUENCHING

Q	$k_Q\tau$ (cm^3)	k_Q (cm^3/s) $\tau \cong 22.2$ n/s
He	9.0×10^{-22} cm^3	4.1×10^{-14}
Ne	7.3×10^{-22} cm^3	3.3×10^{-14}
Ar	1.1×10^{-21} cm^3	5.0×10^{-14}
Kr	1.6×10^{-21} cm^3	7.3×10^{-14}
Xe (2 Body)	6.9×10^{-21} cm^3	3.1×10^{-13}
Xe (3 Body)	2.7×10^{-40} cm^6	1.2×10^{-32} cm^6/s
N_2	1.4×10^{-21} cm^3	6.1×10^{-14}
$C\ell_2$	3.8×10^{-18} cm^3	1.7×10^{-10}
$HC\ell$	2.5×10^{-18} cm^3	1.1×10^{-10}
$CC\ell_4$	3.5×10^{-18} cm^3	1.6×10^{-10}

The Xe measurements exhibited a significant departure from a linear dependence of R vs [Xe] at pressure > 1000 torr as shown in the Stern-Volmer plot of Figure 6. When the Xe data was replotted vs $[Xe]^2$, after subtracting out the two-body dependence, a very good fit to the data was observed, as shown in Figure 7. This indicates that at high pressure there is a three-body quenching channel for Xe on HgCℓ*.

Measurements have also been made for HgBr* quenching to pressures of 1000 torr. The rate constants derived from these studies are listed in Table II. As in the low pressure HgCℓ* case, only an upper bound on the rate constants for the rare gases other than Xe could be determines. The bromine containing molecules show significantly faster quenching rates than the rare gases. As an example, the quenching of HgBr* by CF_3Br is shown in Figure 8. Since CF_3Br optically absorbs at the pump wavelength of 1950 Å, the value of α had to be determined in a separate experiment. This was accomplished by filling the absorption cell (Figure 5) with various pressures of CF_3Br and observing the change in the HgBr* fluorescence in the reaction cell. The ratios I_o/I are displayed on a semi-log plot vs $[CF_3Br]$ in Figure 9. Using a standard Beer's law analysis, the absorption cross section for CF_3Br at 1950 Å was determined as $\sigma = 4.9 \times 10^{-20}$ cm^2. Measurements for the other halides have also been made and are included in Table III. These cross sections have been subsequently checked using a vacuum ultraviolet spectrometer and both sets of measurements were found to be in good agreement.

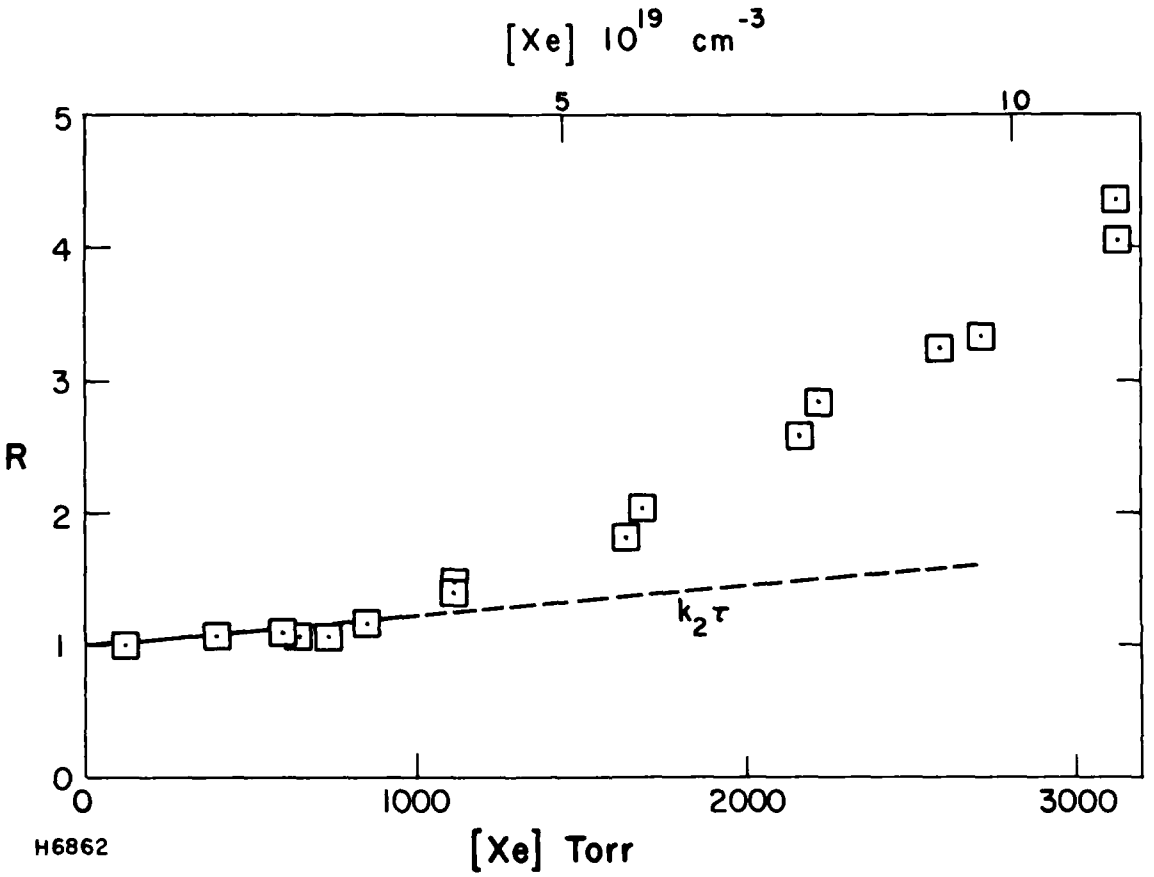

Figure 6 Stern-Volmer Plot for Quenching of HgCℓ* by Xe

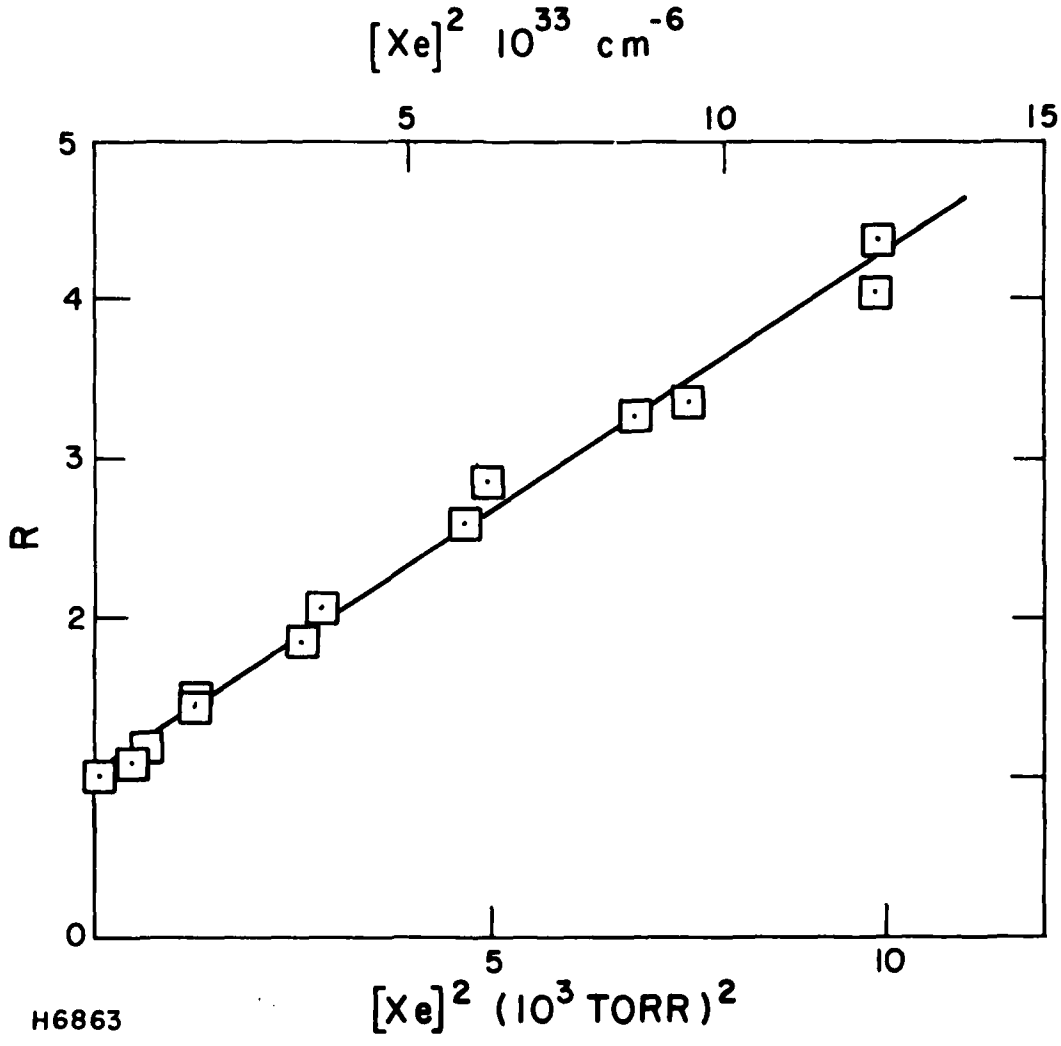

Figure 7 Data of Figure 6 with Two-Body Dependence Subtracted Out Replotted vs $[Xe]^2$

TABLE II

HgBr* ($B^2\Sigma^+_{1/2}$) QUENCHING

Q	$k_Q\tau$ (cm^3)			k_Q(cm^3/s) τ = 23.3 ns Present Exp.
	Present Exp.	Bazhulin, et al.[19]	Eden, et al.[20]	
He	$< 1.5 \times 10^{-21}$	1.3×10^{-21}	11.8×10^{-21}	———
Ar	$< 1.5 \times 10^{-21}$			———
Xe	7.1×10^{-21}	14×10^{-21}	87.7×10^{-21}	3×10^{-13}
N_2	$< 1.5 \times 10^{-21}$	5.5×10^{-21}	104.3×10^{-21}	———
Br_2	6.9×10^{-18}		13×10^{-18}	2.9×10^{-10}
HBr	3×10^{-18}		4.7×10^{-18}	1.3×10^{-10}
CF_3Br	2.1×10^{-18}			8.7×10^{-11}
$CC\ell_3Br$	4.4×10^{-18}			1.8×10^{-10}

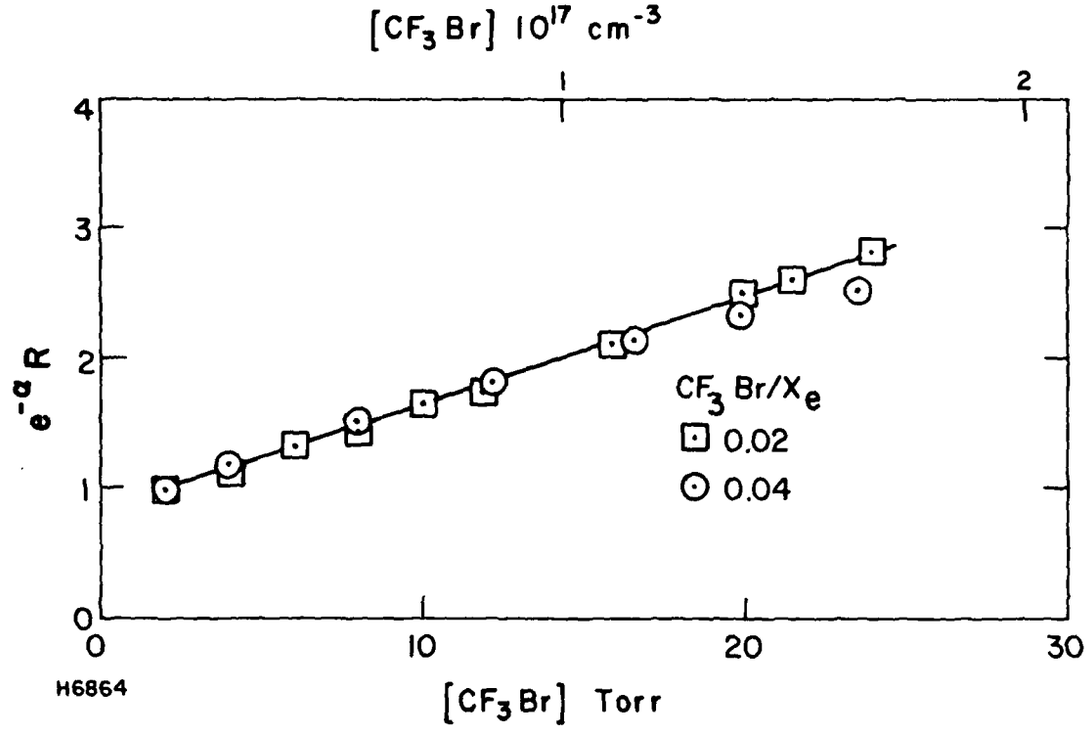

Figure 8 Modified Stern-Volmer Plot for Quenching of HgBr* by CF_3Br

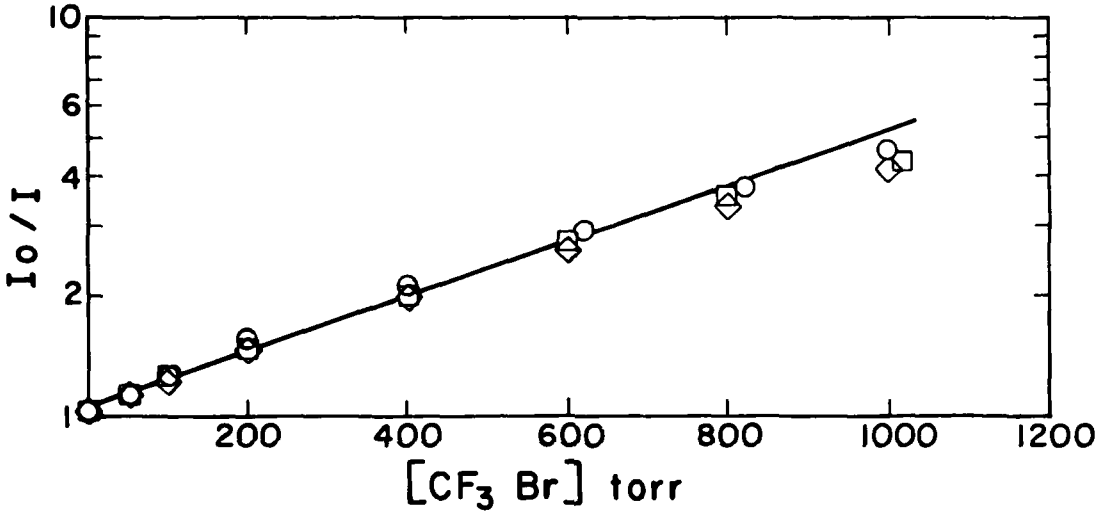

Figure 9 Measured Optical Absorption of CF_3Br in 1 cm Absorption Cell at ~ 1950 Å

TABLE III

ABSORPTION COEFFICIENT, α
(cm^2)

$C\ell_2$	9×10^{-21}	(a)
$HC\ell$	9.3×10^{-19}	(a)
$CC\ell_4$	5.8×10^{-18}	(a)
Br_2	4.2×10^{-20}	(b)
HBr	1×10^{-18}	(b)
CF_3Br	4.9×10^{-20}	(b)
$CC\ell_3Br$	5×10^{-18}	(b)

(a) Value at 1810 Å

(b) Value at 1950 Å

3. Discussion

With the exception of Xe, all the two-body $HgC\ell^*$ ($B^2\Sigma^+_{1/2}$) quenching rates listed in Table I are comparable ($\sim 5 \times 10^{-14}$ cm^3/s) and within our previously[2] determined upper bounds. Xe which is so effective at vibrationally relaxing the B state is also the most effective rare gas quencher of this excited state.

The only measurement in the literature to which one might compare is the work of Tibilow[16] which we have determined indicates a quenching rate constant of $HgC\ell^*$ by $N_2 < 10^{-13}$ cm^3/s. Since our measured rate for N_2 is below Tibilow's detectability, his work is consistent with our measurements. We have included our previously measured rate constants for chlorine containing molecules in Table I for completeness.

From the quenching rate constants given in Table I an estimate of the saturation flux can be obtained for arbitrary mixtures of $Ar/Hg/C\ell_2$ and $Ar/Xe/Hg/CC\ell_4$ which have been used respectively in discharge and e-beam pumping of the $HgC\ell^*$ laser. The quenching of $HgC\ell$ by Hg has recently been measured in a separate experiment[17] as $k_{Hg} = 4 \times 10^{-11}$ cm^3/s. The saturation flux ϕ_s can be computed using the following expression[18]

$$\sigma_s = h\nu/\sigma_s\tau(1 + k_{AC\ell}\,[AC\ell] + k_{Ar}\tau\,[Ar] + k_{Xe}\,\tau[Xe] + k_{Hg}\,\tau\,[Hg]) \qquad (2)$$

where σ_s is the stimulated emission cross section, $h\nu$ is the photon energy, τ is the $HgC\ell^*$ radiative lifetime, and k_i the

quenching rate constant for each component. It should be noted that the saturation flux defined in Eq. (2) is applicable in the limit that the population of the lower laser level is negligible. From the HgCℓ* spontaneous spectra[2] we have estimated $h\nu/\sigma_s\tau$ to be 0.16 MW/cm^2. For typical laser mixes containing 1% $C\ell_2$, 2% Hg and 97% Ar at a total pressure of 2 amagats one obtains ϕ_s = 0.45 MW/cm^2 and for 2% $CC\ell_4$, 2% Hg, 11% Xe and 86% Ar at 2 amagats one obtains ϕ_s = 0.31 MW/cm^2.

The quenching rate constants determined for the HgBr* ($B^2\Sigma^+_{1/2}$) state are listed in Table II. These are lower pressure measurements (< 1000 torr) and, as in the previous[2] HgCℓ* low-pressure quenching work, only upper bounds could be determined for the rare gases and N_2 with the exception of Xe which again is also effective at vibrationally relaxing the upper HgBr* ($B^2\Sigma^+_{1/2}$) manifold. The halogen containing molecules, in this case bromine, are again the most effective at quenching the excited states, exhibiting close to gas kinetic rates.

Two other studies of HgBr* quenching are also cited in Table II. The work of Bazhuline et al.[19] is in reasonably good agreement with our measurements except for N_2 which is about a factor of ~ 3.5 above our upper bound. On the other hand the rates measured by Eden and Waynant[20] appear to be consistantly high. The Xe quenching rate constant is about an order-of-magnitude greater than our measurement and the N_2 quenching rate is almost two orders-of-magnitude higher. However, the faster Br_2 and HBr quenching rates are both within a

factor of two of our values. Since we have taken some care to pump only the HgX* ($B^2\Sigma^+_{1/2}$) state and to vibrationally relax this state, it is a reasonable assumption that any quenching experiment which observes faster rates than ours has inadvertantly includes some additional process, (e.g., quenching by impurities) which increases the observed rate.

All the halogen donor molecules tested absorbed light at the optical pumping wavelength and since these absorption cross sections are necessary in the analysis, they were measured using the 1 cm path length absorption cell shown in Figure 5. The filters used each had a bandpass of ~ 30 nm and these measurements are thus convolutions of the lamp output and the filter bandpass. For cases where the cross section is fairly flat over the filter bandpass we have checked the cross section measurements. For example, the value of the measured HCℓ cross section at ~1800 Å; $\sigma(HC\ell) = 9.3 \times 10^{-19}$ cm^2 is in good agreement with the work of Myer and Samson[21] and the measured value for bromine at 1950 Å; $\sigma(Br_2) = 4.2 \times 10^{-20}$ cm^2 is in good agreement with the value given in Calvert and Pitts[8] at ~ 2000 Å.

C. THEORETICAL STUDY OF FORMATION RATES OF RARE GAS HALIDE TRIMERS

The collisional recombination reaction

$$R_aF^* + R_b + R_c \rightarrow R_aR_bF^* + R_c, \qquad (3)$$

where R_a, R_b, and R_c represent the rare gas atoms Ne, Ar, Kr, and Xe, is important in the kinetics of rare gas fluoride excimer lasers for two reasons. For RF* lasers, this reaction quenches the lasing

molecule RF* and, at the same time, forms $R_aR_bF^*$ which may absorb at the RF* laser wavelengths (e.g., Kr_2F^* absorbs at KrF* wavelengths), resulting in reduced small-signal gain and reduced power extraction efficiency. Therefore, the calculation of rate constants for reactions of the type shown above was performed as part of this contract.

Based on the phase-space theory of Keck and co-workers,[22,23] Shui[24] has recently developed a simple method and calculated the recombination rate constants for the reaction

$$KrF^* + R + R \rightarrow RKrF^* + R \quad (R = Ar, Kr). \qquad (4)$$

The agreement between theory and experiment was about a factor of two. Under this contract, we have calculated recombination rate constants for thirteen reactions of the type represented by Eq. (3). The excimers studies include ArF*, KrF*, and XeF*; the product species include NeXeF*, Ar_2F^*, ArKrF*, ArXeF*, Kr_2F^*, and Xe_2F^*; the third-body collision partners include Ne, Ar, Kr, and Xe.

To calculate rate constants by the phase-space theory it is necessary to have adequate information on the relevant potential energy surfaces. Since complete energy surfaces do not exist for reactions of the type described by Eq. (3), we have used the assumption that any three-body interaction can be described by the sum of the two-body potentials. The relevant two-body interactions (see Ref. 23) involve rare gas dimer ions, fluoride ions and rare gas atoms. Theoretical determinations of the binding energies and equilibrium configurations of the homonuclear rare gas fluorides

are available from several sources.[26,27] Using these data and information available on the binding energies of the heteronuclear rare gas dimer ions,[28] we estimated binding energies for the remaining $R_aR_b^{\pm}$-F^- interactions. The F^---R_c interaction potentials were obtained from the electron gas calculations of Kim and Gordon.[29] The $R_aR_b^{\pm}$-R_c binding energies were estimated from the behavior of the dimer ions and the measured[30] binding energy of Xe_3^+. Table IV summarizes the reactions studied under this contract, together with the key parameters characterizing the interaction potentials. D_{12} refers to the $R_aR_b^{\pm}$-F^- interaction, D_{13} to $R_aR_b^{\pm}$-R_c and D_{23} to R_c-F^-.

As was done in Ref. 24, the recombiantion rate constant can be written as

$$k_r = k_r^B \, (N/N_o)(k/k_e), \tag{5}$$

where N/N_o is a correction factor for the recrossing of the phase-space surface, k/k_e is a correction factor for the nonequilibrium internal energy distribution, and k_r^B is the barrier rate constant given by

$$k_r^B = 4\pi^2 f a^2 z_2^2 \, (z_2 - z_1) \, (8kT/\pi\mu_{XY})^{1/2} \, X[1 - \exp(-B_m/kT)]. \tag{6}$$

Details of the method of calculation have been presented in Ref. 24 and will not be repeated here. However, for the purpose of providing a simple physical explanation for the form of Eq. (6), we may

TABLE IV

REACTIONS, INTERACTION POTENTIAL PARAMETERS, AND RATE CONSTANTS

	Reaction		r_{12}	D_{12}	r_{13}	D_{13}	r_{23}	D_{23}	k_r
(1)	ArF*+Ar+Ar	Ar_2F*+Ar	2.22	0.60	2.48	0.34	2.91	0.114	6×10^{-31}
(2)	KrF*+Ar+Ar	ArKrF*+Ar	2.25	0.46	2.58	0.14	2.91	0.114	2×10^{-31}
(3)	KrF*+Ar+Kr	ArKrF*+Kr	2.25	0.46	2.69	0.73	2.96	0.159	1×10^{-30}
(4)	KrF*+Kr+Ar	Kr_2F*+Ar	2.29	0.60	2.69	0.16	2.91	0.114	3×10^{-31}
(5)	KrF*+Kr+Kr	Kr_2F*+Kr	2.29	0.60	2.79	0.29	2.96	0.159	5×10^{-31}
(6)	XeF*+Ne+Ne	NeXeF*+Ne	2.19	0.05	2.22	0.02	3.12	0.024	2×10^{-33}
(7)	XeF*+Ne+Xe	NeXeF*+Xe	2.19	0.05	2.70	1.00	3.04	0.254	3×10^{-31}
(8)	XeF*+Ar+Ar	ArXeF*+Ar	2.30	0.13	2.71	0.06	2.91	0.114	5×10^{-32}
(9)	XeF*+Ar+Xe	ArXeF*+Xe	2.30	0.13	2.94	0.96	3.04	0.254	8×10^{-31}
(10)	XeF*+Kr+Kr	KrXeF*+Kr	2.33	0.32	2.92	0.10	2.96	0.159	2×10^{-31}
(11)	XeF*+Xe+Ne	Xe_2F*+Ne	2.38	0.60	2.70	0.02	3.12	0.024	3×10^{-32}
(12)	XeF*+Xe+Ar	Xe_2F*+Ar	2.38	0.60	2.94	0.06	3.04	0.114	3×10^{-31}
(13)	XeF*+Xe+Xe	Xe_2F*+Xe	2.38	0.60	3.17	0.27	3.04	0.254	1×10^{-30}

(a) r_{12}, r_{13}, and r_{23} are equilibriumintermolecular distances in 10^{-8} cm; D_{12}, D_{13}, and D_{23} are binding energies in eV; k_r is the recombination rate constant at 300°K in cm^6 $molecule^{-2}$ s^{-1}. See test for discussion on reactions and parameters.

point out that the factor $4\pi z_2^2 (z_2 - z_1)$ is a molecular volume proportional to the number of atom pairs (X-Y) close enough to recombine, wehreas the factor $\pi a^2 (8kT/\pi\mu_{XY})^{1/2}$ is a rate constant proportional to the frequency at which the (X-Y) pairs are stabilized under the influence of the third-body M. The quantity f is the degeneracy factor, and the additional factor $[1 - \exp(-B_m/kT)]$ simply eliminates those atom pairs which cannot form bound molecules because of their excessive orbital angular momentum. A detailed explanation and derivation of these terms are contained in Ref. 23.

The calculated room-temperature rate constants are summarized in the last column of Table IV and are plotted in Figure 10 which shows also the available experimental data[31-36] for comparison. We note that there is considerable scatter in the experimental data where two or more measurements have been reported for the same rate constant. On the average, the agreement between theory and experiment is about a factor of three, over a total variation of rate constants of nearly a factor of 1000. This level of agreement for a large number of reactions indicates that the theory, the method of calculation, and the interaction potential model correctly describes the important features of such reactions. Further refinements and/or improvements can be made by using more accurate potential-energy surfaces and by performing more detailed calculations such as trajectory calculations. Calculations of this type have been discussed in earlier publications[24,25] and can be carried out for the present reactions, if desired.

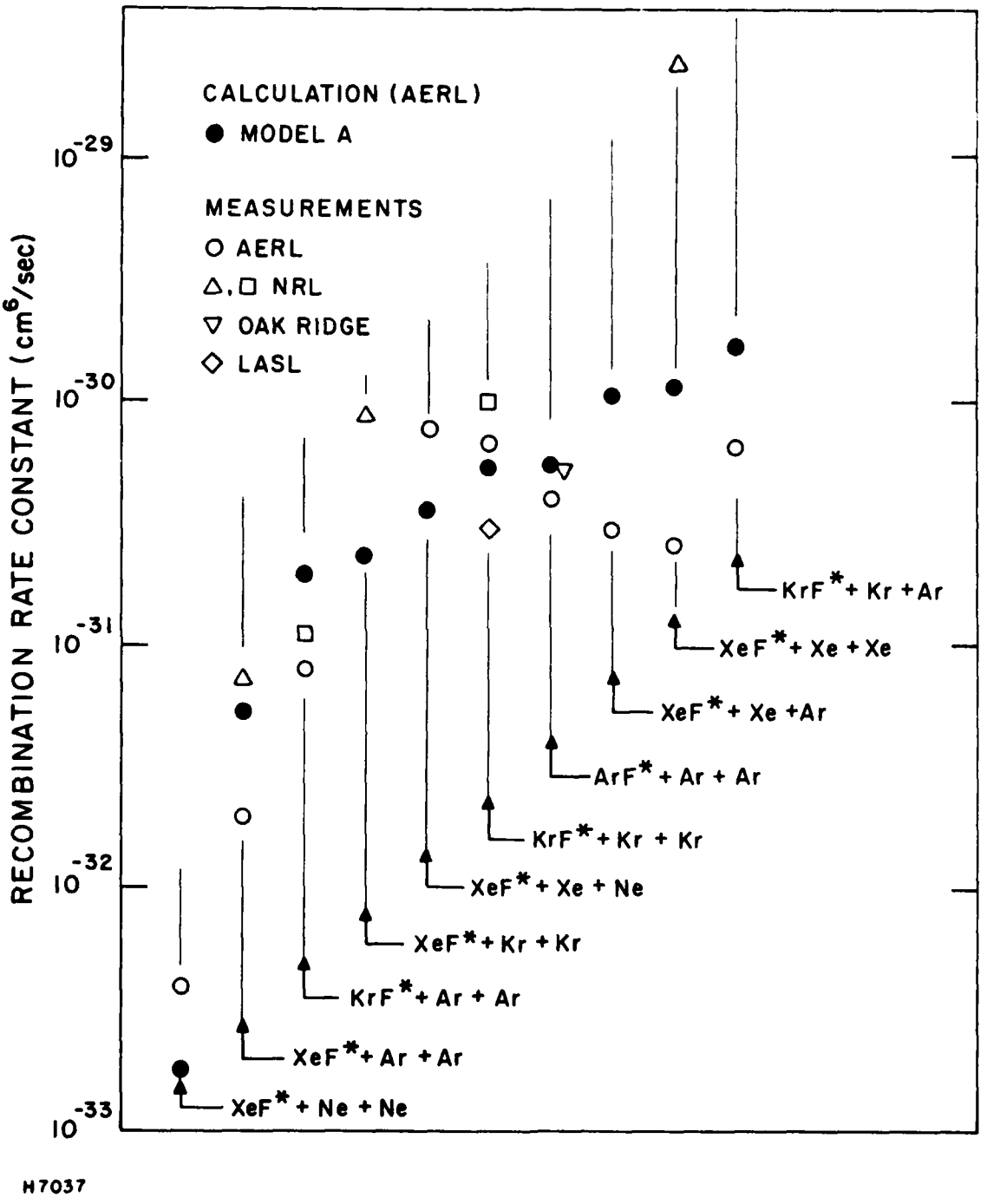

Figure 10 Rare Gas Halide Trimer Formation Rate Constants at Room Temperature

REFERENCES

1. A. Mandl and J.H. Parks, Rev. Scientific Instrun 50, 127 (1979).

2. A. Mandl and J.H. Parks, App. Phys. Lett. 33, 498 (1978).

3. See for example, J.J. Ewing, "Excimer Lasers," to be published, Laser Handbook, M. Stitch, editor, North Holland (1979).

4. J.H. Parks, App. Phys. Lett. 31, 192 (1977).

5. J.H. Jacob, J.A. Mangano, M. Rokni and B.N. Srivastava, Bul. Amer. Phys. Soc. 23, 147 (1978); K.Y. Tang, R.O. Hunter, Jr., J. Oldenettel, C. Houston, D. Heustis, D. Eckestrom, B. Perry and M. McCusker, App. Phys. Lett. 32, 226 (1978); W.T. Whitney, App. Phys. Lett. 32, 239 (1948).

6. J. Hsia and J.H. Jacob (to be published), 1979.

7. An. N. Nesmeyanov, "Vapor Pressure of the Elements" (Academic, New York, 1963).

8. J.G. Calvert and J.N. Pitts, "Photochemistry," Wiley, New York, 1966 and Reference within.

9. From Figure 3, $\frac{I_{before}}{I_{after}} = \frac{8}{9} = e^{-n\sigma\ell}$. For $\sigma = 1 \times 10^{-12}$ cm^2 and $\ell = 10$ cm, this absorption can be explained by $\sim 1 \times 10^{10}$ atoms/cm^3 of residual mercury.

10. See for example, J. Crank, "The Mathematics of Diffusion," Oxford University Press, 1967.

11. For example, 3.5×10^{17} $HgCl_2$ molecules fromed in a 50 cm^3 vessal of surface area 90 cm^2 could form virtually several hundred monolayers on the surface.

12. K. Wieland, Zeit. f. Phys. 76, 157 (1932).

13. J. Maya, J. Chem. Phys. 67, 4976 (1977); Appl. Phys. Lett. 32, 365 (1978).

14. J.G. Eden, Appl. Phys. Lett. 33, 495 (1978).

15. N. Djeu and C. Mazza, Chem. Phys. Lett. 46, 172 (1977).

16. S. Tibilow, Acta Physchim. U.S.S.R. 7, 171 (1937).

17. J.H. Parks and D. Klimek, (AERL) (Unpublished).

18. W.W. Rigrod, J. Appl. Phys. 36, 2487 (1965).

19. S.P. Bazhulin, N.G. Basov, et al., Kvantovaya Elektronika 5, 684 (1978).

20. J.G. Eden and R.W. Waynant, paper presented at Gaseous Electronics Conference, Buffalo, NY, October, 1978.

21. J. Myer and J.A.R. Samson, J. Chem. Phys. 52, 266 (1970).

22. J.C. Keck, Adv. Chem. Phys. 13, 85 (1967).

23. V.H. Shui, J.P. Appleton and J.C. Keck, J. Chem. Phys. 53, 2547 (1970).

24. V.H. Shui, Appl. Phys. Letters 31, 50 (1977).

25. V.H. Shui, J. Chem. Phys. 57, 1704 (1972).

26. W.R. Wadt and P.J. Hay, J. Chem. Phys. 68, 3850 (1978).

27. D.L. Huestis and N.E. Schlotter, J. Chem. Phys. 69, 3100 (1978).

28. C.Y. Ng, P.W. Fiedemann, B.N. Mahan and Y.T. Lee, J. Chem. Phys. 66, 5737 (1977).

29. Y.S. Kim and R.G. Gordon, J. Chem. Phys. 61, 1 (1974).

30. H. Helm, Phys. Rev. A 14, 680 (1976).

31. M. Rokni, J.H. Jacob, J.A. Mangano, R. Brochu, Appl. Phys. Lett. 31, 79 (1977).

32. J.G. Eden, R.W. Waynant, J. Chem. Phys. 68, 2850 (1978).

33. C.H. Chen, M.G. Payne and J.P. Judish, J. Chem. Phys. 69, 1626 (1978).

34. M. Rokni, J.A. Mangano, J.H. Jacob, J.C. Hsia, IEEE J. Quantum Electron QE-14, 464 (1978).

35. G.P. Quigley, W.M. Hughes, Appl. Phys. Lett. 32, 627 (1978).

36. J.G. Eden, R.W. Waynant, S.K. Searles and R. Burnham, Appl. Phys. Lett. 32, 733 (1978).

DISTRIBUTION LIST

Director, Advanced Research Projects Agency 1400 Wilson Boulevard Arlington, Virginia 22209 Attention: Program Management	2 copies
Scientific Officer	3 copies
Administrative Contracting Officer	1 copy
Director, Naval Research Laboratory, Attn: Code 2627 Washington, D.C. 20375	6 copies
Office of Naval Research Department of the Navy Arlington, Virginia 22217 Attention: Code 102IP	6 copies
Defense Documentation Center Bldg. 5, Cameron Station Alexandria, Virginia 22314	12 copies
Office of Naval Research Branch Office - Boston 495 Summer Street Boston, Massachusetts 02210	1 copy